JOURNAL OF PROPULSION AND POWER
Vol. 18, No. 2, March–April 2002

Time- and Length Scales of Combustion in Liquid Rocket Thrust Chambers

B. Ivancic* and W. Mayer†
DLR, German Aerospace Research Center, D-74239 Lampoldshausen, Germany

This paper summarizes experimental and computational results of research on propellant mixing and combustion in high-pressure LOX/GH2 rocket combustors. Hot-fire tests and numerical experiments are utilized to get more detailed information about the physics of mixing and combustion under high-pressure (transcritical) conditions. Time- and length scales of the reacting shear layer are identified by results from numerical simulation and experiments. The comparison between numerical and experimental results show the same tendencies of the distribution of length scales within the reactive shear layer. It was ascertained that the length scales are increasing downstream of the injector face plate. Qualitative and quantitative data about the flowfield (morphology, velocity, species distribution, etc.) at different boundary conditions are presented.

Nomenclature

D	=	diameter, thickness
Da	=	Damköhler number
I	=	intensity
K	=	correlation factor
Ka	=	Karlovitz number
k	=	turbulent kinetic energy
L, l	=	length scale
$\dot{m}$	=	mass flow
T	=	temperature
t	=	time
V	=	velocity
x	=	axial position
Y	=	species mass fraction
ε	=	turbulent dissipation rate
λ	=	wave length
μ	=	dynamic viscosity
ρ	=	density

Subscripts

c	=	chamber
chem	=	chemical
exp	=	experimental
init	=	initialization
inj	=	injector
int	=	integral
kol	=	kolmogorov
P1, P2	=	Pixel1, Pixel 2
sim	=	simulation
w	=	window

Introduction

THE research during the last few years on liquid oxygen (LOX)/gaseous hydrogen (GH_2) injection, mixing, and combustion has led to a more profound understanding of the processes in a cryogenic rocket engine combustion chamber.[1–4] Some basic phenomena of propellant injection, mixing, and combustion are well understood, though the knowledge is still not satisfactory in view of quantitative assessment of part processes, for example, turbulent mixing and combustion of the propellants. To investigate the interaction between the mixing and combustion process, the knowledge of their time- and length scales is imperative. To study these processes in hot-fire tests under representative conditions (real-gas effects at supercritical conditions and high Reynolds numbers), numerical simulations and experiments were performed, and the results are compared.

Experimental Setup

Hot-fire tests in a subscale combustor with optical access (Fig. 1) have been performed. The combustor has a modular design, which makes it possible to change the axial position of the windows. Thus the flow phenomena can be observed from the injector plane up to 430 mm downstream. This windowed combustor was constructed for chamber pressures up to 10 Mpa. Earlier tests were done with a single shear coaxial injector at chamber pressures of 3 MPa (Ref. 1). In this publication the results of the latest experiments with a chamber pressure of 6 MPa are presented. In Fig. 2 and Table 1 the geometrical and the injection boundary conditions are listed. The windows are protected from the hot combustion gases by a circumferential H_2 purge flow. This cooling film also has the function to simulate the influence of neighboring injector elements. The windows have a size of 100×25 mm.

Flow-visualization techniques such as single-shot shadowgraphs (Fig. 3) and OH-/H_2O-imaging (Fig. 4) were utilized to visualize the flow and flame structure. The OH emission was detected in a wavelength range of $\Delta\lambda = 300$–310 nm (spectra of LOX/GH2 flames are published in Ref. 4), and the emission of the hot H_2O vapor was detected in a wavelength range of $\Delta\lambda > 530$ nm. The gate of the charge-coupled device (CCD) camera was adjusted to 100 ns, and the frequency of the single shots was 50 Hz.

Experimental Results

The shadowgraphs shown in Fig. 3 are subdivided in three parts, each with a length of 30 mm. The shadowgraphs point out that the jet is still intact at the end of the optical access, 100 mm downstream from the injector. The dense oxygen jet exhibits large surface perturbations. The shadowgraphs reveal a flow phenomenology of the LOX jet, which is similar to a fluid/fluid mixing process.[2,3] No ligament or droplet formation can be observed.

The chamber pressure of 6.0 MPa is higher than the critical pressure of oxygen (5.04 MPa). The injection temperature (see Table 1) is close to the critical mixing temperature of 152.6 K at 6.0 Mpa for H_2/O_2-systems.[5,6] The heat transfer of the flame to the oxygen

Presented as Paper 99-2211 at the 35th JPC, Los Angeles, CA, 20–23 June 1999; received 23 October 1999; revision received 30 May 2001; accepted for publication 17 September 2001.

*Aerospace Engineer, Space Propulsion.
†Head Propellant Injection Research, Space Propulsion. Senior Member AIAA.

jet increases the temperature to the critical mixing temperature at the interface of the oxygen jet. This interface has a jagged surface and high density gradients. The mixing takes place between a dense (oxygen) and a light fluid (hydrogen and combustion gases) in a turbulent reactive shear layer.

The OH and H2O emissions (Fig. 4) are a line-of-sight view. The images reveal that the flame is attached at the LOX post.[4] The flame-holding mechanism in the wake of the LOX post is apparent. Because of the very thin reactive shear layer in the injector near region and the broadening of the shear layer downstream, the emission intensities of OH and H2O are rising with increasing distance from the face plate. Starting at a distance of about 30 mm from face plate, the mean intensities seem to remain constant.

Simulation

In addition to the experiments, numerical simulations were performed by the computational fluid dynamics (CFD)-Code Aeroshape 3D, which includes the standard k–ε model for turbulence. The combustion is modeled with the assumption of chemical equilibrium. Properties of oxygen are modeled using a real-gas approximation. Aeroshape 3D is an explicit finite volume solver, which works on quasi-unstructured grids.[7] The numerical mesh has 150,000 cells, and the grid is adaptive to the solution. The injection conditions of the simulation are set to measured values from the experiment (see Table 1). The inflow conditions of the turbulence values (k, ε) are assumed as fully develloped turbulent pipe flow with a turbulence intensity of $Tu = 10\%$.

The calculation was steady-state and two-dimensional. In these computations the solution reached full convergence after 680,000, iterations which includes some mesh-refinement loops. Figure 5 shows an example of the results of the numerical simulation.

The hydrogen jet and therefore the flame bends in the near-injection zone. One can obviously see these effects as well as the broadening of both the oxygen jet and the reactive shear layer (Fig. 5). The velocity of the hydrogen jet decreases very rapidly, whereas the oxygen jet velocity remains nearly constant over a distance of about 200 mm downstream.

Principal Analysis of Flow

The results of the numerical simulations were compared with the experimental results to identify discrepancies. These discrepancies

Table 1 Geometrical data and injection conditions

Geometrical data			Injection conditions		
D_c	50 mm	T_{LOX}	127 K	ρ_{LOX}	956.08 kg/m^3
D_{LOX}	4 mm	TH2, inj	125 K	$\rho_{H2,inj}$	11.68 kg/m^3
t_{mat}	0.3 mm	TH2, purge	293 K	$\rho_{H2,purge}$	5.00 kg/m^3
D_{inj}	6.5 mm	$\dot{m}_{LOX}$	0.30 kg/s	V_{LOX}	24.97 m/s
t_w	1.0 mm	$\dot{m}_{H2,inj}$	0.06 kg/s	$V_{H2,inj}$	310.2 m/s
D_{throat}	16.8 mm	$\dot{m}_{H2,purge}$	0.23 kg/s	$V_{H2,purge}$	300.07 m/s

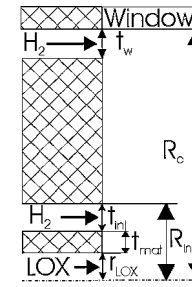

Fig. 2 Geometry of face plate.

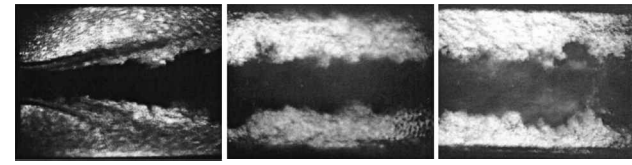

Fig. 3 Shadowgraphs of injected oxygen jet in a hot-fire test at chamber pressure of 6 MPa.

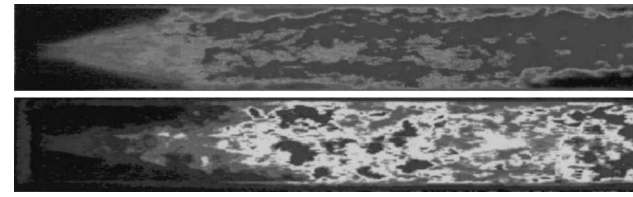

Fig. 4 OH-imaging single shot (upper picture) and H_2O-imaging single shot (bottom picture) at a chamber pressure of 6 MPa.

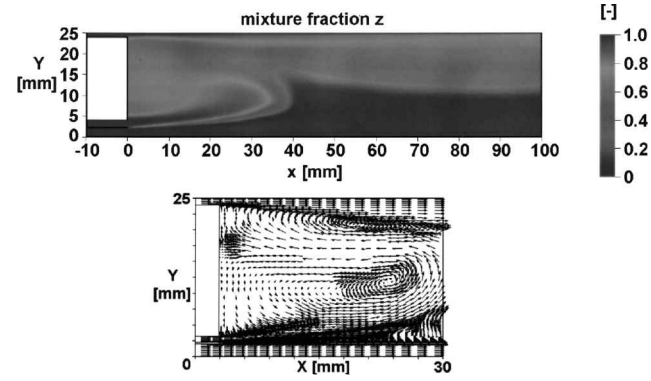

Fig. 5 Mixture fraction Z (upper picture); velocity vector plot (bottom picture).

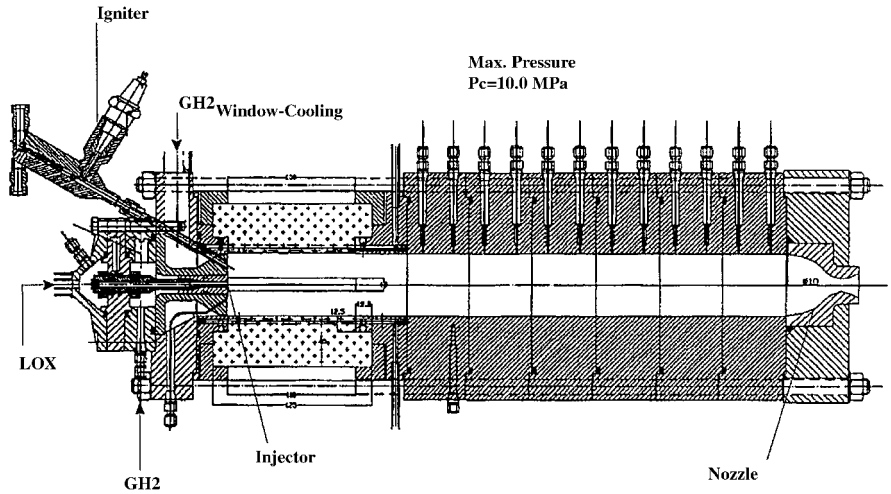

Fig. 1 Windowed single-injector model combustor.

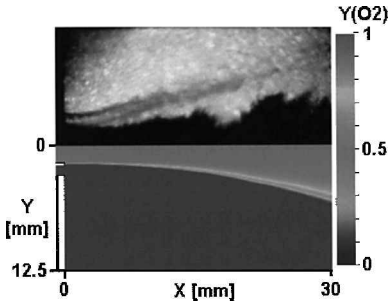

Fig. 6a Shadowgraph (upper picture); oxygen mass fraction (bottom picture).

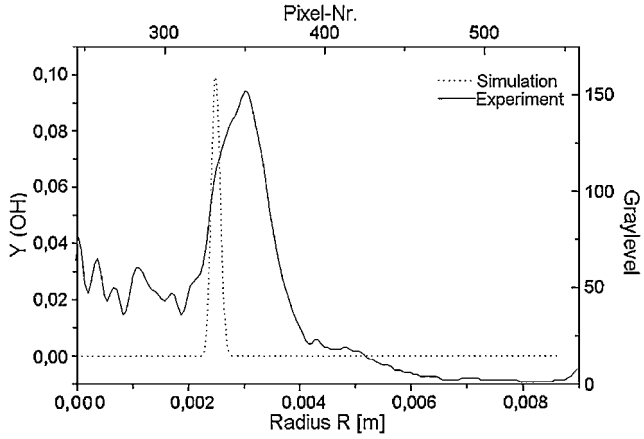

Fig. 6b OH distribution (cross section 10 mm downstream).

identified weak points of the physical models in the CFD code. Figure 6a shows the phenomenological comparison between a shadowgraph picture of the oxygen jet in the near-injector region (from face plate up to 30 mm downstream) and the calculated oxygen mass fraction in the same region. One can observe the expansion of the oxygen jet. As the numerical simulation is steady-state, the instationary surface perturbations, which are seen in the experiment (for example, see shadowgrahs in Fig. 4), are not resolved. These large-scale surface perturbations (no turbulence phenomena) are caused by flow instability phenomenas, and their interaction to the reactive shear layer can in principle not be resolved by turbulent steady-state simulations. Figure 6b shows a comparison of the radial OH distribution at an axial position of 10 mm downstream from injector. The experimental OH distribution is yielded by the Abel transformed OH-imaging picture. The OH-emission intensity data were deconvoluted using an Abel transformation to produce a two-dimensional cross section through the centerline of the OH-intensity distribution. The Abel transformation assumes cylinder symmetry of the flame. Because the single shots (see Figs. 3 and 4) are nonsymmetrical, 200 pictures were summed together, and a time-averaged picture from these 200 single shots was calculated. These averaged images are cylinder symmetrical, and the Abel transformation can be applied. The OH regions, which are measured experimentally and then transformed by the Abel procedure, represent the mean OH distribution in a cross section averaged over all single shots. Therefore the Abel-transformed OH intensities are influenced (that is, broadened) by the large-scale instability and turbulence fluctuations. The broadening caused by turbulence fluctuation is in principle resolved by the stationary solution of the numerical simulation (k–e turbulence model). The difference is only that the average of the experiments is taken over 200 single shots and a steady-state simulation represent a theoretical average for $t \rightarrow \infty$. The principle discrepancy in the comparison of a steady-state solution of a numerical simulation and experimental results are large-scale flow instability phenomena, which influence the instantaneous position of the reactive shear layer. For this reason, the comparison of the OH distribution in Fig. 6b is shown at an axial cross section of 10 mm downstream from injector. In this near-injector region it is assumend that the large-scale instability effects can be neglected. This assumption is supported by the shadowgrahs (for example, see Fig. 4), where one can see that the large-scale fluctuations start after approximately 20 mm downstream from the injector. In Fig. 6b the left Y axis with the OH-mass fraction is only valid for the numerical simulation. The experimental data are measured in gray levels (right Y axis), and therefore it is only a qualitative OH distribution. Two major discrepancies are visible in this diagram. The thickness of the OH zones is not simulated correctly, and the radial distance of the OH zones to the centerline is different between calculation and experiment. As just mentioned, one reason for these discrepancies is assumed to be the simplified steady-state, two-dimensional calculation, which cannot resolve correctly the transient three-dimensional processes.[8,9] But these effects are not dominant in the near-injector region. Here the main reason for the discrepancies is the very simple combustion model (infinite fast chemistry model $\Rightarrow$ chemical equilibrium), which does not take into account interactions between chemistry and turbulent mixing.

The intensities of the experimental OH distribution between the centerline ($R = 0$ mm) and the radial position of $R = 2$ mm are unrealistic because here the oxygen jet is existent. These intensities are artifacts of the numerical instabilities of the mathematical Abel procedure and the noise of the original single-shot images.

Investigation of Timescales

To investigate the interactions between turbulence and combustion, it is very important to know the timescales at which the relevant processes occur. A characteristic time for turbulence should specify the velocity of the turbulent mixing and a timescale of the chemistry, characterizing the speed of the pure chemical kinetics. Comparing these timescales, one can deduce various interaction mechanisms between turbulence and chemistry (broading of flames, wrinkling, etc.).[10] Unfortunately, the reality is much more complicated. Both the turbulent processes and the chemical processes do not have one distinct timescale. There is a spectrum of timescales for the flow turbulence and for the chemistry depending on local conditions. This problem is discussed in the next two sections.

Turbulent Timescales

The turbulence theory assumes that the turbulent processes occur over a wide range of length and timescales. Turbulence is produced on large scales. In this context the integral turbulent timescale is very important as it represents the scale of the turbulent structures with the highest turbulent energy. This scale does not represent the largest turbulent scale but is in the same order of magnitude. At the bottom end of the turbulent cascade where the turbulent energy k dissipates to heat, the Kolmogorov scales are relevant. The integral t_{int} and Kolmogorov t_{kol} timescale are defined as follows.

$$t_{\text{int}} = k/\varepsilon, \qquad t_{\text{kol}} = \sqrt{\mu/(\rho \cdot \varepsilon)}$$

Figure 7 shows these two turbulent timescales. Between these two scales the most important turbulent processes are taking place. Both scales are given at every local point by the results of the numerical simulation. In the upper picture of Fig. 7, the near-injector region is displayed. Here the influence of the shear layer is very strong.

Increasing the distance to the injector, the intensity of the shear layer becomes weaker and finally disappears. The timescales are decreasing very rapidly in the shear layer. In the regions where the velocity gradient is very high, the timescale decreases very fast in the direction of the high velocities. In the bottom picture (axial distance to the injector is greater than 100 mm) a relaxation of the large gradients takes place, and the timescales are almost constant over the radius. One can see that the turbulent range between the integral and the Kolmogorov timescales comprises 1–2 orders of magnitude. The smallest Kolmogorov timescales have the magnitude of 1 μs in the reactive shear layer. It is indispensable to compare these turbulent timescales with the chemical timescales in order to investigate the interaction mechanisms between turbulence and chemistry.

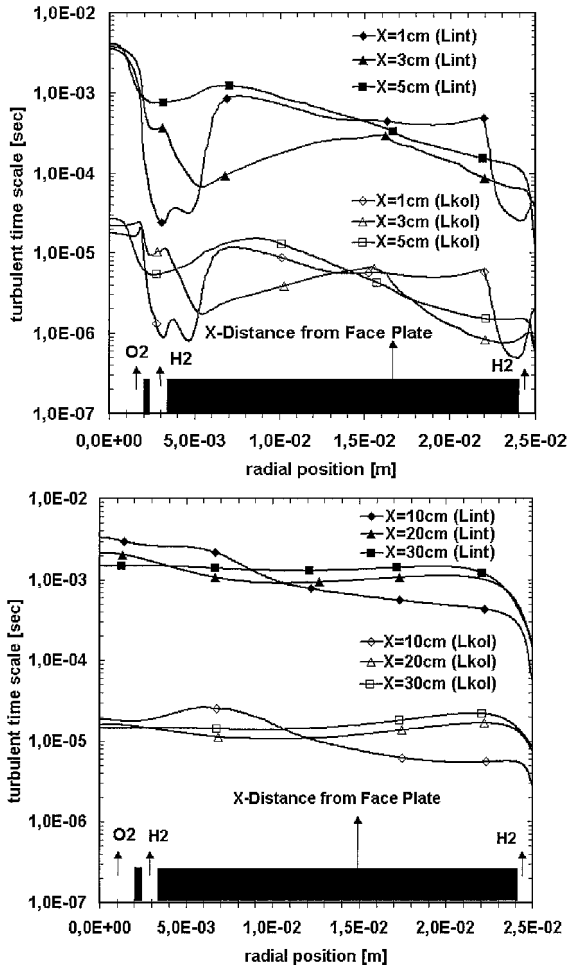

Fig. 7 Radial distribution of turbulent timescales at different axial positions: top—near-injector region ($X < 50$ mm: influence of shear layer is visible); bottom—far downstream region ($X > 100$ mm: influence of shear layer has disappeared).

Chemical Timescales

In this section the pure chemical kinetic processes are discussed separate from the turbulent flow. It is assumed that the combustion process in rocket combustion chambers occurs under adiabatic and isobaric conditions. Figure 8 shows exemplary the kinetic transients of an adiabatic, isobaric combustion process with an initial temperature of 2000 K and a system pressure of 6 Mpa (This high initial temperature and pressure of the reactands H_2 and O_2 result in the very high adiabatic flame temperature of approximately 4000 K.).

In this study the chemical equilibrium is defined when the system temperature (adiabatic flame temperature) attains 99% of the equilibrium adiabatic flame temperature. In Fig. 9 a parametric study is presented for several different initial conditions (initial temperature, stoichiometric mixture). The time this system needs to reach chemical equilibrium is calculated for various pressures.

The parametric study of the initial mixture ratio reveals a weak dependency over a wide scope (ROF: 3–13) in view of the time that the system requires to reach equilibrium. This statement is of course not true when the difference of the initial mixture ratio to the stoichiometric mixture ratio is too large (ignition conditions). Figure 9 represents the chemical timescales for stoichiometric initial mixtures. Regarding the chemical timescales, it is evident that the dependency on the initial temperature is very strong, particularly for high pressure. Therefore it is necessary to explore the temperature of the propellants in the reactive shear layer. Depending on mixing temperatures of the propellants, the velocity of chemical reaction is determined, and one can see for relevant temperatures the turbulent and chemical timescales can be of the same order of magnitude.

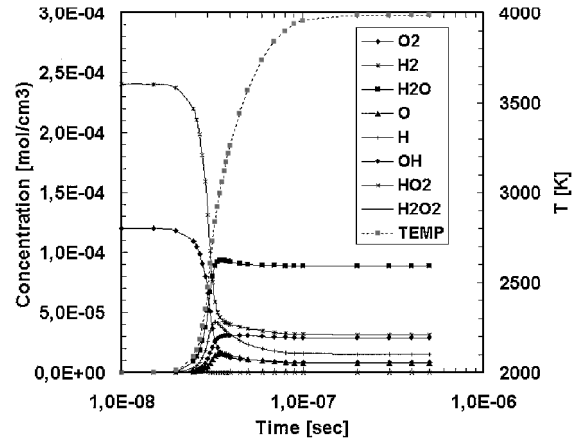

Fig. 8 Detailed kinetic mechanism.

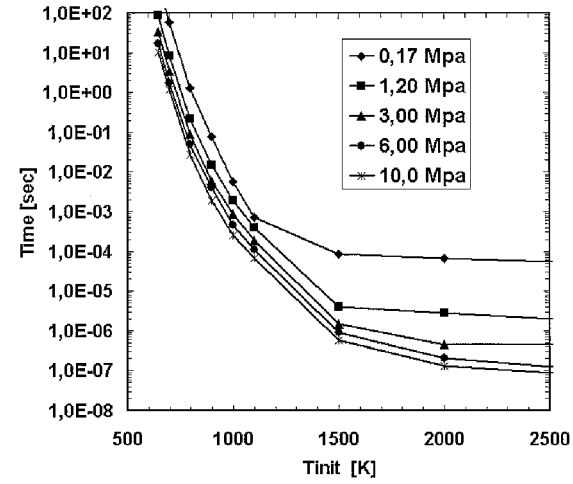

Fig. 9 Chemical timescales for various system pressures.

Investigation of Length Scales

In addition to the timescales, another very important variable to characterize turbulent combustion processes are the relevant length scales. This experimental study can determine coherent structures and their respective length scales. The OH-emission pictures in the near-injector region are used to extract relevant turbulent length scales. To accomplish this task, the following assumption must be made: The visible coherent structures of the OH emissions are correlated with the coherent structures of turbulent flow. The evaluation procedure of theses length scales will be elucidated now more in detail.

The experimental data set is comprised of OH intensities detected by an 8-bit CCD camera with an exposure time of 100 ns and a frequency of 50 Hz. In these experiments the near-injector region is detected with a heightened resolution. The detection area starts at the injector plane and goes to 30 mm downstream. This range is resolved by the CCD camera with 577 pixels (1 pixel = 0,04 mm). The local resolution is within the turbulent spectrum. Of course, one cannot resolve the smallest (Kolmogorov) but the larger turbulent structures. In the original images (gray values) every pixel has intensities between 0 (black) and 255 (white). These images represent a projection of the three-dimensional OH intensities on a plane (line of sight).[11] For this reason, the evaluation of the length scales are calculated based on the intensities on the symmetry line. Only at these points it is ensured that the detection direction is perpendicular to the reactive shear layer. Figure 10 illustrates this approach. This graphical representation shows an example of an OH single shot with its symmetry line. On the right-hand side a sketch is shown, which represents a cross section at the axial position of A-A. The intensities detected by the CCD camera at an arbitrary pixel on the symmetry line represent a signal, which is the sum over the radial

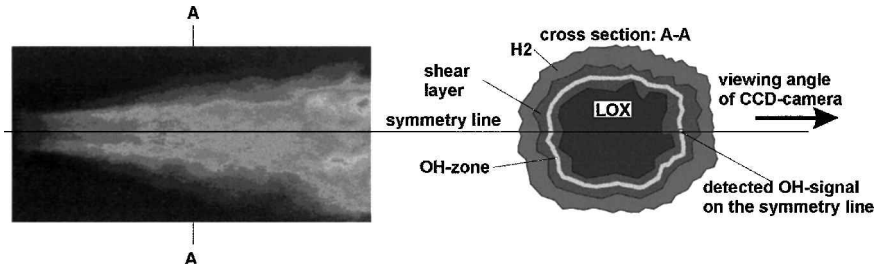

Fig. 10 OH single shot and phenomenological sketch of cross section at axial position A-A.

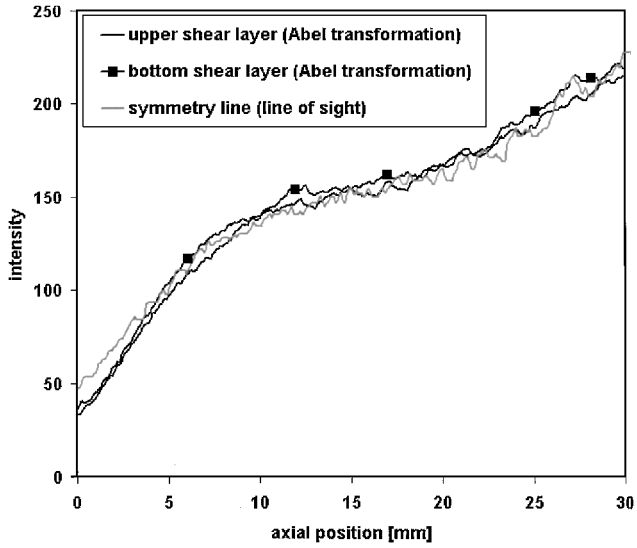

Fig. 11 Comparison of axial OH distributions (symmetry line) and Abel-transformed shear layer.

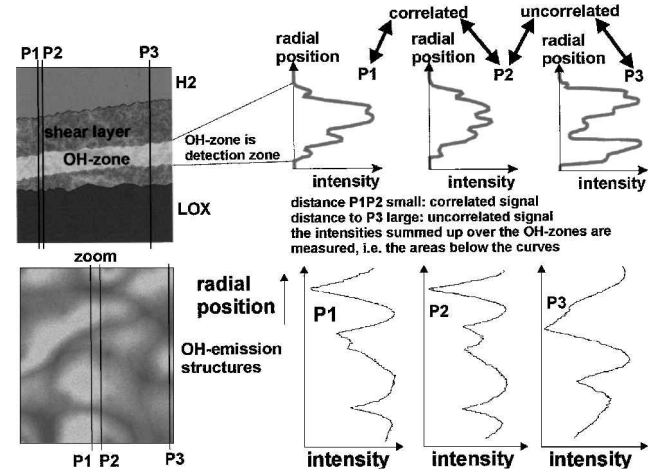

Fig. 12 Phenomenological sketch and OH-intensity distribution in the reactive shear layer.

thickness of the OH zones (combustion zones) within the reactive shear layer. In the near-injector region OH only exists within the reactive shear layer. This can be proven by a comparison of the axial intensity distribution of OH emissions on the symmetry line and the OH emissions extracted from Abel transformation in the following diagram.

The intensities of the Abel-transformed pictures (Fig. 11) represent the radial summation through the OH zones (averaged over all single shots) in the reactive shear layer at various axial positions. Both the upper and the lower shear layer were calculated. The curve that represents the intensities of the symmetry line is averaged over all single shots, too. One can recognize obviously that the OH intensities on the symmetry line correlate with the intensities summed over the radial thickness of the Abel-transformed OH emissions within the reactive shear layer. It is therefore obvious that the detected OH emissions on the symmetry line in the near-injector region come only from the OH radicals produced within the combustion zone. Within these combustion zones the investigation of coherent structures using the well-known two-point correlation method is discussed now. Figure 12 shows the phenomenology underlying this evaluation procedure. The coherent structures in this model are considered vortices. They represent the turbulent coherent structures as well as the OH-emission structures. By the application of the two-point correlation method, the length scales of these coherent structures are determined. The length scales extracted in this manner represent an average over the OH thickness in the reactive shear layer (see Fig. 12). Therefore, mean length scales of coherent OH structures, which are correlated with turbulent structures, are determined (averaged over the radial combustion zone thickness within the shear layer).

For the evaluation procedure an intensity profile over all single shots is ascertained for every pixel on the symmetry line. Because the images are detected with a frequency of 50 Hz, the single shots are statistically independent. This frequency corresponds to an interval of 0.02 s between two sequential single shots. Comparing this interval with the numerically simulated timescales, one can recognize the interval between the single shots is much larger than the highest turbulent timescale. So every single shot can be regarded as a statistically independent measurement. For two OH signals of neighboring locations, the two-point correlation method is utilized by calculating a correlation factor with the following formula:

$$K_{P1,P2} = \frac{\overline{I'_{P1} \cdot I'_{P2}}}{\sqrt{\overline{I'^2_{P1}}} \cdot \sqrt{\overline{I'^2_{P2}}}}$$

To determine this correlation factor for two neigboring points $P1$ and $P2$, one needs the rms values of the intensity fluctuations I' at both points and also the average of the correlation $I'_{P1} * I'_{P2}$. If these data are measured, one knows all variables for calculating the correlation factor as shown in the equation. This factor describes the degree of correlation between the two points. The correlation factor has the maximum value of one. This is applied when the two measuring points are identical ($P1 = P2$). In this case the signals are fully correlated. Increasing the distance between these two points, the correlation factor approaches zero. It is also possible that the correlation factor has negative values, and in normal cases at certain distances between two points the factor is negative (minimum value is approximately $-0,2$). When the distance between two points get larger than the largest turbulent structures, then the two measured intensities get fully uncorrelated ($K \approx 0$). The next step is to investigate the dependency of the correlation factor to the distance between two points by producing a graph of the factor K over the distance. With this graph it is possible to make predictions of the relevant length scales in the reactive shear layer. In Fig. 13 a representative theoretical correlation curve is shown. This curve makes it possible to calculate various relevant length scales. One of the most popular

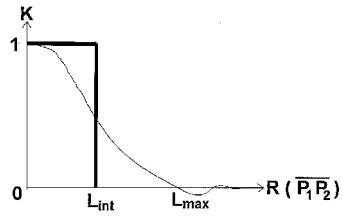

Fig. 13 Theoretical dependency of correlation factor K on the distance $P1P2$.

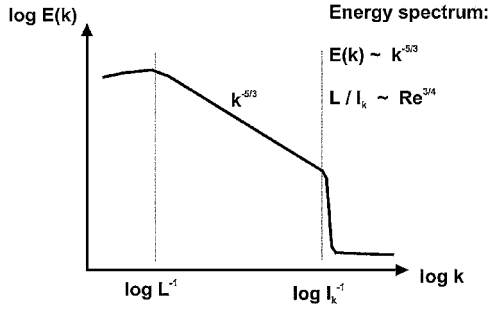

Fig. 14 Turbulent energy cascade with relevant length scales.

is the length scale indicated in Fig. 13. The integral length scale is calculated by the following equation:

$$L_{\text{int}} = \int_0^{\infty} K_{(R)}\, \mathrm{d}R$$

L_{int} specifies the integral length scale and corresponds to equal areas under the curve and the rectangle. In turbulence theory this scale plays an important role because it is assumed the vortices with this scale contain the most energy within the turbulent energy cascade (see Fig. 14). The two turbulent length scales bounding the inertial range of turbulence are the integral and the Kolmogorov length scale, which are defined as follows:

$$L_{\text{int}} = k^{\frac{3}{2}}/\varepsilon \qquad l_{\text{kol}} = (\mu^3/\rho^3\varepsilon)^{\frac{1}{4}}$$

In this study the length scale calculated by the integral over the correlation factor K is not used because of the expensive numerical effort to calculate this integral for every point on the symmetry line. Here a length scale is utilized, which is very close to the integral and very easy to calculate. It is the length scale when the correlation factor K has the value of 0, 5. By means of some exemplary studies, it was ascertained that the difference between the integral length scale and the length scale, which is used in this study, is smaller than 5%. So it is justifiable that the additional expenditure to calculate the exact integral length scale does not remunerate. In this framework a program was developed calculating the correlation factors and length scales for every pixel on the symmetry line (taking into account arbitrary numbers of single shots).

From this data set we can extract 577 correlation curves. Comparing these curves, one can recognize they broaden downstream. This shows the relevant length scales increase with increased distance from the injector plane.

In Fig. 15 these length scales (defined as the distance when $K = 0, 5$) from the experimental data set are shown with the numerically simulated length scales. The integral and Kolmogorov length scales calculated by AS3D (see equations for L_{int} and l_{kol}) are displayed in Fig. 15 from the injector plane ($X = 0$ mm) to 30 mm downstream ($X = 30$ mm) as well. The radial location is where the OH concentration is maximum.

Comparing the numerically simulated length scales with the length scales of the OH correlations, one can see the connection between the OH-emission structures and structures of turbulent flow. The experimental length scales lie between the integral and the Kolmogorov length scale of simulation but closer to the integral length scale.

As already mentioned, for the flame emission pictures the Abel transformation was performed, and in Fig. 16a it is shown that this

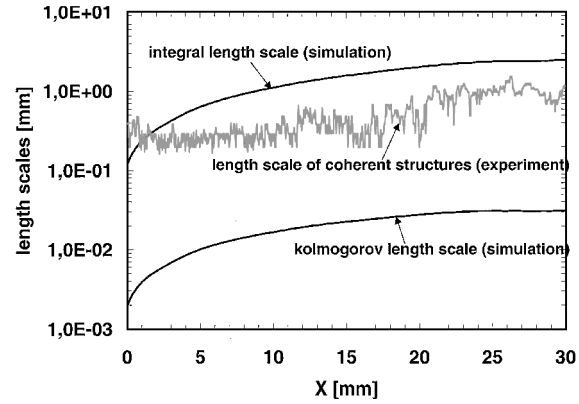

Fig. 15 Comparison between numerical simulated length scales and the correlated length scales.

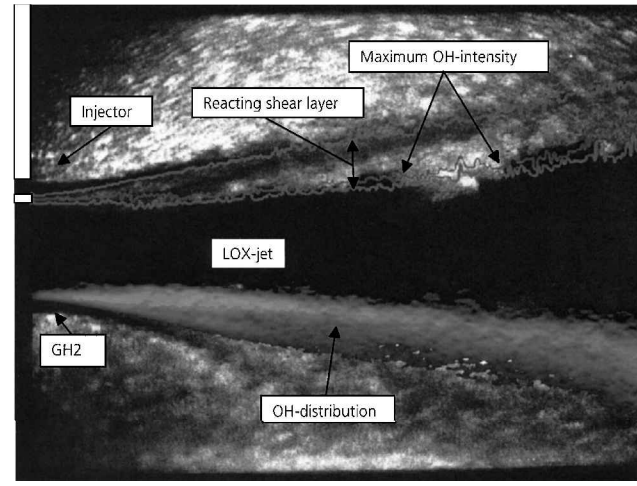

Fig. 16a Shadowgraph with OH regions.

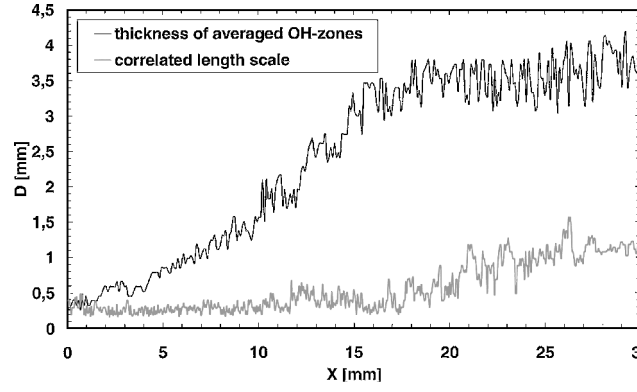

Fig. 16b Thickness of averaged OH zones and length scales for OH correlations.

makes it possible to measure the thickness of the OH zones over the average of all of the single shots. It is assumed that this mean OH zone represents the region where the reactive shear layer occurs as a result of the turbulent fluctuation and in particular as a result of the large-scale flow instability fluctuations. In Fig. 16a a shadowgraph together with the deconvoluted OH regions is shown. In the upper branch of the OH zones, the interfaces (blue lines) and the maximum OH-intensity line (red line) are displayed (the interface lines are defined as 5% of the maximum OH intensity). The reason why the interface is not on the surface of the LOX jet at every position is the shadowgraph is an instant picture, and the OH regions are averaged over 200 single shots. The shadowgraphs show a very intensive fluctuation of the LOX interface (caused by turbulence

and flow instability fluctuations). The diagram in Fig. 16b exhibits the thickness of the averaged OH zones computed in this manner together with the correlated length scales.

The thickness of the averaged OH zones is increasing very rapidly after their formation at the LOX post. At 30 mm downstream from injector, the OH zone has a thickness of approximately 4 mm, which is four times higher than the measured length scales within the reactive shear layer. In this regard the instant shear- layer thickness plays an important role. The shear-layer thickness is comparable with the pipe diameter in a pipe flow. This scale represents the largest possible length scale. The averaged OH zones represent the positions where combustion occurs. This zone is broadened by averaging over the single shots caused by turbulent and flow instability fluctuations. It is obvious that the flow instability phenomena and the radial turbulent fluctuations, which are responsible for the broadening of the OH zones, are decreasing in the direction of the injector (for example, see shadowgraphs in Fig. 3). Therefore, in the near-injector region to approximately 20 mm downstream, the thickness of the OH zone is comparable with the instant shear-layer thickness. At these locations one can compare the correlated lengths scale, which remains nearly constant in the first 10 mm downstream with the evolution of shear-layer thickness, which is increasing right from the injector.

Conclusions

The length scales of the turbulent flow are investigated experimentally and numerically. The spectrum of length scales represents the structures, which are determining the turbulent mixing process. It was ascertained by numerical investigation that the Kolmogorov length scale is in the magnitude of 1μm at the injector exit plane and is increasing downstream. The integral turbulent length scale is at every point almost two orders of magnitude higher. The experimentally measured length scales are in the same order of magnitude and show similar tendencies. These quantified length scales represent the sizes of the turbulent structures within the reactive shear layer. The shear-layer thickness was quantified, too. In the injector plane the shear layer is established, and its thickness is from roughly LOX-post thickness (that is, 0, 3 mm) increasing to a value of approximately 4 mm at the axial position of 20 mm downstream.

To investigate the interaction mechanism between turbulence and chemistry in the reactive shear layer, it is, besides the length scales, also important to quantify the timescales of the turbulent and chemical processes. Comparing the speed of the mixing process with the speed of the chemistry, one can deduce the turbulent combustion regime at a local position. In this study timescales of turbulent mixing and combustion processes are quantified; thereby, the smallest turbulent mixing time (the Kolmogorov timescale) has the magnitude of 1 μs in the reactive shear layer, very close to the injector. The integral turbulent timescale at this location is approximately 20 μs. Because the velocity gradients at the reactive shear layer are declining downstream, the turbulent timescales are increasing within the reactive shear layer, and consequently the radial profile is equalized. At 30 cm downstream the Kolmogorov and the integral timescales are almost constant over the whole diameter of the combustion chamber ($t_{kol} \approx 20\,\mu$s, $t_{int} \approx 1$ ms). Comparing the studied flow and chemical timescales, one can derive that various interaction mechanisms between flow turbulence and chemistry are possible. It seems different combustion regimes (for example, see Borghi[10]) occur in the reactive shear layer of a coax injector flow.

Acknowledgments

This work is supported in the frame of the "German National Technology Programme Cryogenic Rocket Engines," TEKAN, under Contract 50TT9628. The authors thank the P8 test bench team for realization of the hot-fire tests.

References

[1]Mayer, W. O. H., Ivancic, B., Schik, A., and Hornung, U., "Propellant Atomization and Ignition Phenomena in Liquid Oxygen/Gaseous Hydrogen Rocket Combustors," *Journal of Propulsion and Power*, Vol. 17, No. 4, pp. 794–799, 2001.

[2]Mayer, W. O. H., Schik, A., Vielle, B., Chauveau, C., Gökalp, I., Talley, D. G., and Woodward, R. D., "Atomization and Breakup of Cryogenic Propellants Under High-Pressure Subcritical and Supercritical Conditions," *Journal of Propulsion and Power*, Vol. 14, No. 5, 1998, pp. 835–842.

[3]Mayer, W. O. H., Schik, A., Ivancic, B., and Krülle, G., "Atomization and Combustion of Cryogenic Liquids at High Pressure," *Proceedings of the 13th Annual Conference on Liquid Atomization and Spray Systems*, ILASS, July 1997.

[4]Mayer, W. O. H., Schik, A., and Schäffler, M., "Injection and Mixing Processes in High-Pressure Liquid Oxygen/Gaseous Hydrogen Rocket Combustors," *Journal of Propulsion and Power*, Vol. 16, No. 5, 2000, pp. 823–828.

[5]Candel, S., Herding, G., Snyder, R., Scouflaire, P., Rolon, C., Vingert, L., Habiballah, M., Frisch, F., Pealat, M., Bouchardy, P., Stepowski, D., Cessou, A., and Colin, P., "Experimental Investigation of Shear Coaxial Cryogenic Jet Flames," *Journal of Propulsion and Power*, Vol. 14, No. 5, 1998, pp. 826–834.

[6]Mayer, W., Tamura, H., "Propellant Injection in a Liquid Oxygen/Gasous Hydrogen Rocket Engine," *Journal of Propulsion and Power*, Vol. 12, No. 6, 1996, pp. 1137–1147.

[7]Gavriliouk, V., and Odintsov, J., "AS3D-M Technique Description," Comp. Aerodynamics Systems Co., Rept. 01.01.33C-96, 1996.

[8]Stoukov, M., Vandrome, D., and Hieu Ha Minh, H., "Direct Numerical Simulation and Modelling of Two-Phase Jet Flows," *Third French-German Colloquium*, Research on Liquid Rocket Propulsion, Universite de la Mediterranée, June 1997.

[9]Villermaux, E., and Hopfinger, E., "Instability Mechanism in Liquid/Gas Shear Layers," *Third French-German Colloquium*, Research on Liquid Rocket Propulsion, Universite de la Mediterranée, June 1997.

[10]Borghi, R., "Turbulent Combustion Modelling," *Progress in Energy and Combustion Science*, Vol. 14, 1988, pp. 245–292.

[11]Moser, M. D., Merenich, J. J., Pal, S., and Santoro, R. J., "OH-Radical Imaging and Velocity Field Measurement in a Gaseous Hydrogen/Oxygen Rocket," *29th Joint Propulsion Conference and Exhibit*, AIAA 93-2036, June 1993.